Starshade Challenge Report **4/2/22**

PI: Dr. Angelle Tanner (MSU)
co-PI: Dr. Joseph Carson (CofC)
Student: Claire Geneser (MSU)
Student: Aly Nida (CofC)

1. Introduction

This report is meant to summarize the analysis of the simulated Starshade images provided as part of the JPL Starshade Challenge. The images were produced with the SISTER tool (Hildebrandt et al. 2022) which incorporates the Starshade PSF, any visible glint from the Sun reflecting off of the Starshade, the light from the exoplanet and emission from zodiacal light, exozodiacal light from debris disks and background stars and extended emission. In addition to simulated science images, we were provided a cube of model PSFs. Each image in the cube represents a model of the PSF at a range of star distances from the geometric center of the Starshade ranging from 0 to 150 mas. Based on the information provided by JPL, we can expect a variation on the Starshade alignment of up to 14 mas. We were also provided a file containing the expected transmission of a point source also at a range of distances of 0 to 150 mas from the Starshade center to be used to correct the amount of light coming from an object which is partially covered by the Starshade.

We can expect that all the Starshade science targets will be vetted, prioritized, and well characterized prior to observing. While we were not provided the location or brightness as a function of passband of the planet candidates, we were given the name of the host star. Upon the real-world investigation of these systems with the Starshade, we should know the degree of the exozodi light coming from the system from its spectral energy distribution (SED) and may have some idea of the morphology, extent, and emission levels of the disk via long wavelength images from ALMA, Spitzer, or Herschel. While these images may give us an estimate of the inclination and extent of the dust, we will still not know everything about the close-in dust morphology or the degree of asymmetry in the outer extents. In this report a sub-set of the simulated images are analyzed using a few different approaches. In addition, we discuss improvements that can be made to our analysis if given more time to work on the simulated data as well as how we might approach a real-world data set.

Solar image glint is caused by light from our Sun reflecting off the Starshade. It has a somewhat distinctive signature, at least in the simulated data, as two bright spots on opposite sides of the Starshade. This is an unlikely pattern produced by planets but could be somewhat reproduced by an edge on disk. In that case it is still emission which would need to be modeled and removed to characterize any planets in the frame. We note that based on studies of the expected glint properties, these contributions to the Starshade images are not truly Gaussian in shape. The best practice for a real-world imaging program would be to collect images of stars with no known observable planets or exozodiacal light (mature stars) to build up a set of glint model standards.

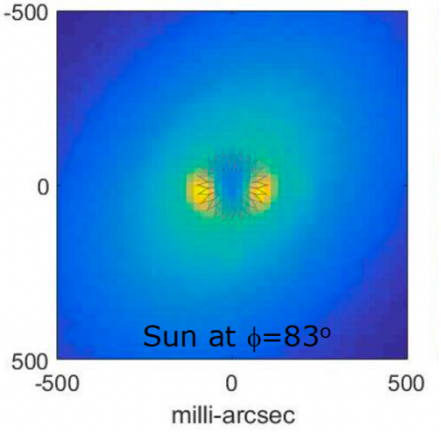

Figure 1: An example of glint from the SISTER simulations. A subset of the simulated images appears to have similar features but upon closer inspection are more likely edge-on disks.

2. Analysis

Over the course of this program, we utilized three main techniques to characterize and then remove light from the image which is not associated with the planet. The techniques employed include: 1) PSF subtraction, 2) disk modeling and, 3) multi-epoch differential imaging. PSF subtraction involves subtracting a model or PSF in the absence of any apparent exo-zodical emission to better reveal the faint emission from the planetary point source. Disk modeling is used to create a simple model of any circumstellar emission present in the image for a single epoch. Once the model is made, it is subtracted from the science image leaving emission from the planet. Multi-epoch subtraction is the method of using two different epochs we will assume that the planet will have changed its position angle while any circumstellar disk emission remains stable. To characterize what type of analysis needed to be performed on each image, an initial by eye inspection was performed. For those images which appeared, by eye, not to have any extended emission near the Starshade, an additional analysis of comparing the profile of an image slice through the position of the star with a similar slice of the model centered PSF was performed. If there was a contribution of some extended emission, this image was slated for additional disk modeling to better remove this emission prior to analysis of the emission from the planet. An example of this component of the analysis is given in Figure 2. A more thorough determination could also be done by subtracting a PSF from the image and highlighting though which significant residual emission.

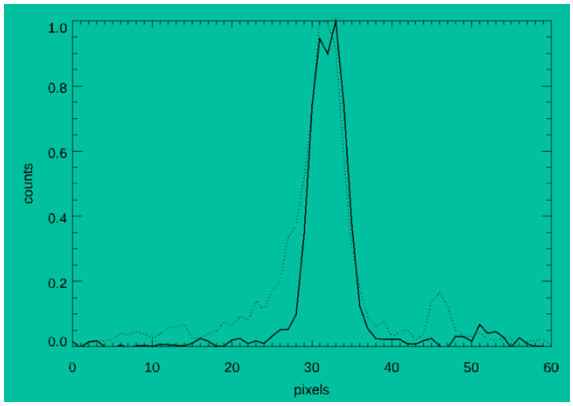

Figure 2: Plot of two slices through the center of the images of tau Ceti. The solid line shows an example of an image with no visible extended emission while the dotted line shows the same slice through another simulation which did show a small amount of extended emission in addition to the PSF.

3. Results

With 700 simulated images to choose from we are going to highlight a select few of the simulated images to demonstrate how we handled multiple characteristics of the simulated images in addition to determining whether planets were present. Below we look at some of these images and address our best methods for address these signals.

3.2 Images with Planets and Little Exozodiacal Light

When vetting Starshade targets, attention will be paid to choosing those known planetary systems with anticipated low levels of exo-zodiacal light based on intense studies of their SEDs. In these cases, we hope that the resulting Starshade image will consist primarily of the Starshade PSF and a point source contribution from the planet. In this simple scenario, the image should be analyzed using the provided Starshade PSF cube which can be utilized to remove the light from the PSF. We can iterate through each image in the cube first normalizing the Starshade PSF to have the same level of light contribution as that seen in the image, shifting the Starshade PSF to make sure its properly centered to the one in the image and then subtracting that PSF from the image. The success of the fit to the data is determined from an estimate of the standard deviation of the pixels within a circle of radius 3 pixels to not include flux from the planet. We then iterate through all the Starshade PSFs in the cube and choose that PSF which produces the most complete subtraction. We performed such an analysis on the simulated image of tau

Ceti which contained a zodi = 1 contribution of light from zodiacal emission at the position of the Starshade (see Figure 3). The image shows clear emission from a point source at PA = 0 and no visible contribution of appreciable zodiacal light. The image also shows no extended emission when stretching the image background which would indicate dust emission at large separations. Figure 3 shows a clear signal from the Starshade PSF and a point source with little to no visible exo-zodiacal light. We discuss the subsequent determination of the properties of the planet in Section 3.4. For the real-world mission scenario, the best approach would be to perform this type of analysis and then also determine the degree of emission remaining after the PSF+planet fit and subtraction compared to other parts of the image for an assessment of the degree of zodiacal light present.

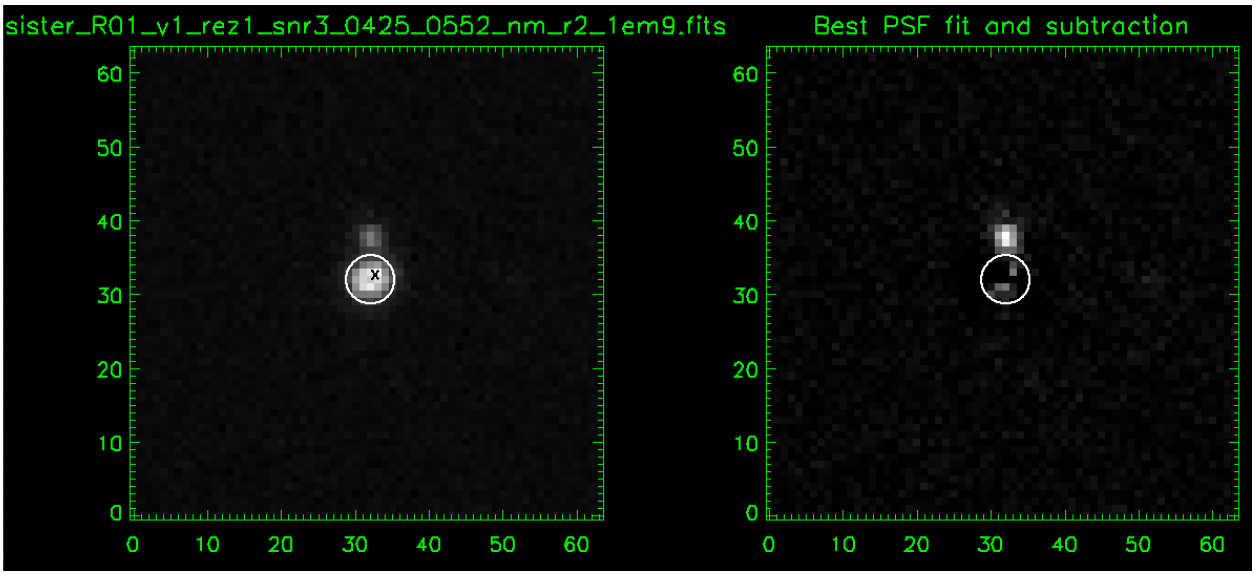

Figure 3: Left - Image of tau Ceti (SNR Level 3, Sim R01, 425-553nm. rez1) which appears to have primarily a PSF (point source) contribution. Right – same image after subtraction of the PSF.

3.3 Using Differential Imaging for Planet Detection

Using separate epochs or image rotations to attempt to subtract out the light from the PSF while using a coronagraph has been a common planet-search technique since Hubble (Lowrance et al. 2005). With the HST NICMOS images, two images were collected with a roll of 30 degree between. As a result, the PSF pattern remained stationary while any faint point source would have a component of angular motion. The subtraction of the two images would remove a degree of the PSF and leave a positive/negative hint of faint point source emission if present. This technique was called roll differential imaging. In the absence of a roll maneuver, the simulated data provided for this challenge did come with two separate epochs of data. In this scenario, we rely on the natural orbital motion of any bound planets to move the point source emission while keeping the PSF and any extended emission stationary. Similarly, the subtraction of the two images should remove everything except a positive/negative point source of planetary emission. There may be only a single point source if the planet was fully behind the Starshade using one of the epochs.

The variety of circumstellar emission present in the simulated images has led us to the conclusion that using differential imaging is an ideal method to search for planetary emission. This aspect of the research completed for this data challenge was led by co-I Dr. Joseph Carson who employed a summer student to complete some initial analysis. The investigation focused on two epochs of the tau Ceti data set, for one

single wavelength range (615-800 nm) and high signal-to-noise (SNR Level 3). We chose this set as our test example because the tau Ceti system is well characterized (e.g. well known inclination angle, disk shape, etcetera) and the planet was detectable in individual "raw" images by visual inspection for both epochs (see Figure 4). This reduced the number of unknowns when trying to evaluate results.

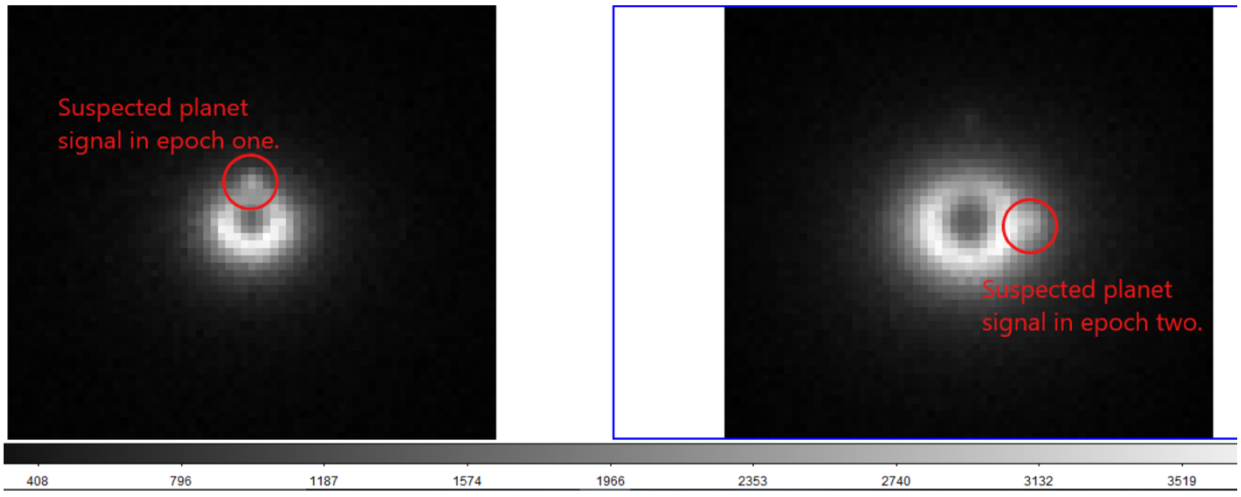

Figure 4: Tau Ceti (SNR Level 3, Sim R01, 615-800nm) as viewed in two epochs, after normalizing for exposure time. Even without processing, a candidate exoplanet can be seen in both epochs.

Th Carson team employed a few different strategies to model the emission from the disk.

Strategy 1: Use the software package *diskmap* (https://pypi.org/project/diskmap/) to model the disk in a single epoch and digitally subtract the modeled disk. As long as the disk light can be modeled as separate from the exoplanet light, a disk-free final image should result where the exoplanet can be detected.

Strategy 2: Use *diskmap* to model the disk based on one epoch data, and then subtract the modeled disk from the other epoch data. This approach serves as a variation on Strategy 1.

Strategy 3: Implement an optimized subtraction of the Epoch 1 data set from the Epoch 2 data set, ideally resulting in a disk-free differential image with a positive and negative planet signal remaining.

Strategy 1 failed to enable exoplanet detection, due to the exoplanet self-subtracting. This occurred because *diskmap* modeled the exoplanet point source as effectively being a part of the disk. With *diskmap* failing to model the exoplanet as separate from the disk, Strategy 2 failed to generate useful results. With the exoplanet exhibiting orbital motion between epochs, Strategy 3 successfully provided an effective method for enabling the exoplanet detection. As shown in Figure 5, the exoplanet signal from Epoch 1 and Epoch 2 can be detected at high signal-to-noise. The exoplanet signal from Epoch 1 is 39% larger than the exoplanet signal from Epoch 2 (1.05 counts/sec versus 0.75 counts/sec). This observed change in brightness is presumably due to a change in planet phase.

Strategy 3 did indeed enable a robust detection of the exoplanet point source in both epochs. However, if a resonant disk structure were to have a similar orbit, it could be mis-identified as an exoplanet, barring a spectroscopic analysis that might differentiate the two celestial phenomena. The detection of both the positive and negative planet flux (representing the Epoch 1 and Epoch 2 positions) helps confirm that the exoplanet detection is real, as opposed to being a random speckle occurring in one

epoch's data. The dual detection also enables a measurement of orbital motion. Changes in planet flux between epochs make comparing the two detections more complicated because [a] one cannot check for identical brightness to confirm that one is seeing the same celestial source in both epochs, and [b] the fainter flux could potentially go undetected in one epoch. A final drawback of orbital differential imaging is of course that it cannot be applied to a single epoch of data.

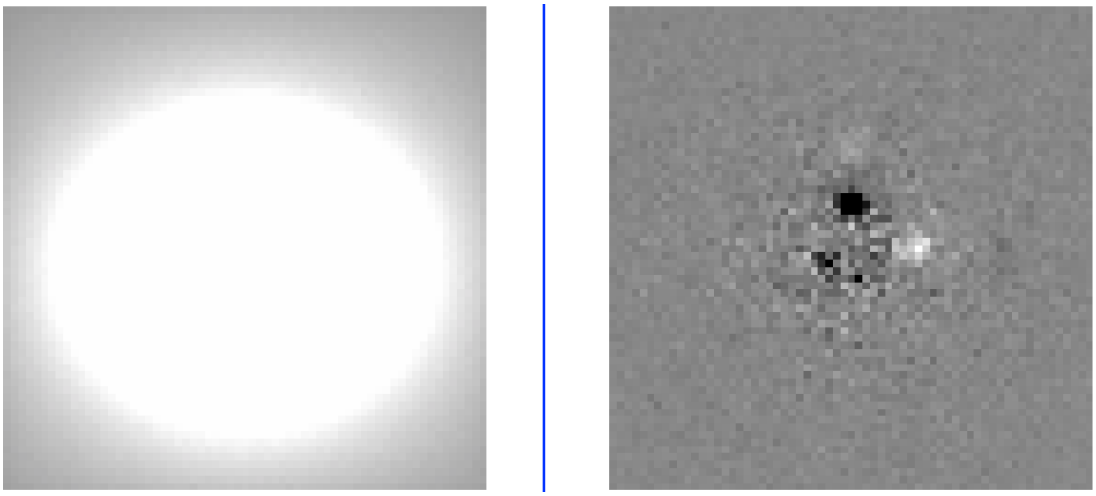

Figure 5: tau Ceti (SNR Level 3, Sim R01, 615-800nm) as viewed with identical scaling settings before (left tile) and after (right tile) subtracting Epoch 1 from Epoch 2. (Before subtraction, data sets were normalized and median-combined.) The negative and positive planet fluxes, corresponding to Epoch 1 and Epoch2 orbital positions, can be easily identified in the right tile at high signal-to-noise. The change in planet brightness between the two epochs is presumably due to a change in planet phase.

With the results of the Carson team, we use this differential method on a few different simulations covering different stars, planet configurations and circumstellar emission. Figure 6 shows the difference images from the R02, R03, R04, R05, R06 and R10 sets which include Tau Ceti, eps Indi, Beta Cvn, and Sig Draconis. The disk emission included face-on, edge-on and in between. In all cases there is clear positive small scale emission remaining although the distance of the point sources from the IWA varies and some systems with multiple planets do not necessarily have emission from both planets in each epoch. Some of the images including the center frame have point sources which are close enough to the IWA to warrant a flux adjustment due to attenuation from the Starshade. While these images had integration times which resulted in the same planet SNR per epoch, it would be more prudent to keep the integration times the same in both epochs to ensure a complete extended emission subtraction. This assumes that the disk flux does not change between epochs. Also in a real-world scenario, planet identification will be aided by a priori information of the orbital properties of the planets which radial velocities and/or Gaia astrometry. In those cases where the planet orbit has been identified with astrometry, we will know where the planet should be therefore allowing us to best schedule the observations or investigate that part of the image more thoroughly. Ideally, we would schedule the observations to coincide with the largest star-planet separation. For some systems, this still may result in the planet being close to the IWA given a small semi-major axis or a large system distance.

3.4 Characterizing the Planets

To characterize the planets, we employed two different methods: 1) aperture photometry and, 2) PSF fitting. For the aperture photometry we use an aperture of 2.5 pixels with a sky annulus of 3 to 4 pixels in

the 425-552 nm images. The same radii were used for the 616-800 nm images. The location of the planet was determined with the IDL centroid function. In all cases the planet flux and position were determined post PSF and/or disk emission subtraction. When using PSF fitting, we used a 2-D gaussian to model the point source emission from the planet. In this case two sets of iterations were performed, one to determine the best fitting position of the planet and another to determine the best scale factor. The best fits were determined via the smallest degree of standard deviation in the pixels within a radius of 2.5 pixels from the position of the planet. Initial guesses to both the position and flux of the planet were used from the aperture photometry and centroid values. Once the best PSF and the location of the planet are estimated, then we perform a simultaneous fit of the PSF and the planet to the image while iterating on the scale of the two contributions to produce a more robust estimate of the flux of the planet.

Figure 6: A menagerie of difference images of multiple simulations with various disk geometries and planetary configurations. This image is to demonstrate that this multi epoch difference strategy is a simple yet effective method for removing extended emission near the inner working angle. Note that for some of these images, the point source emission is on the edge of the Starshade (see white circle in center frame) requiring an additional flux adjustment to account from some attenuation from the edge of the shade. This is performed in the planet analysis section, 3.4.

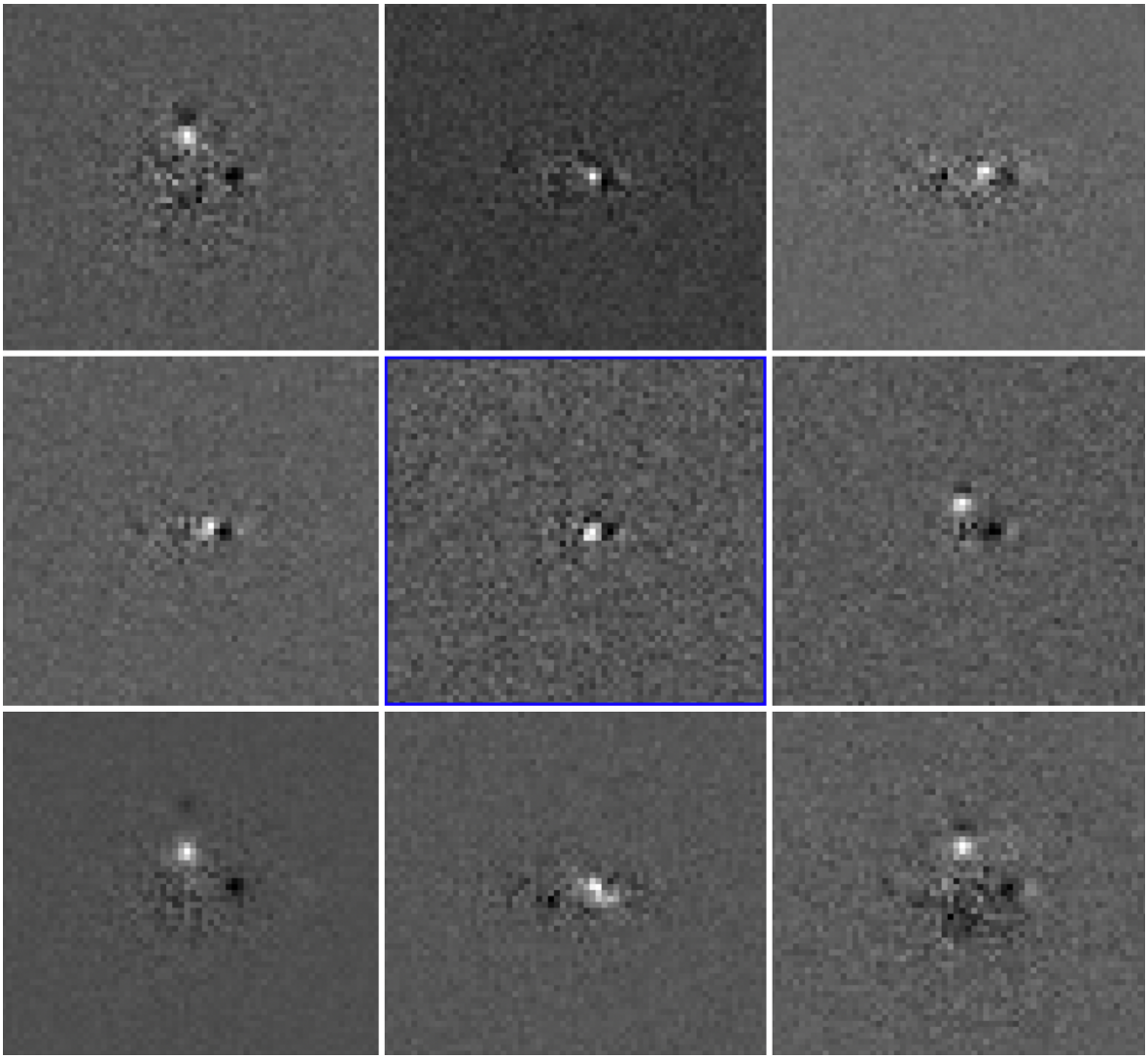

Table 1 includes the properties of the planets detected in images with no discernable exo-zodi emission. These simulations serve as a good test for the accuracy of our planet flux code in the absence of background emission. There are two columns for the planet/star ratio – the first is from the aperture photometry and the second is from PSF fitting. For those images with exo-zodi dust, the planetary properties were determined after subtraction of both the combination of the Starshade and the dust emission. Table 2 includes the properties of planets for which the extended emission was removed using the via-epoch subtraction method. The photometry of the planet is determined via the same aperture photometry as for those sources with no visible extended emission. For the simulations we analyzed, some of the planets were close to the inner working angle. For these scenarios, we used the provided Starshade transmission curve. To estimate we flux correction factor, we interpolated the value based on the curve provided and its separation in mas from the center of the Starshade (center of the image).

Table 1: Planet properties for those images with no visible exo-zodi emission

					Aperture	PSF Fit		
Planet Properties Filename	**Planet #**	**Position Ang [o]**	**Separation [mas]**	**SNR**	**Flux Ratio**	**Flux Ratio**	**Wavelength nm**	**Epoch**
sister_R01_v1_rez1_snr1_0425_0552_nm_r2_1em9	1	0	129.0	1	3.68E-09	4.06E-09	425-552	1
sister_R01_v1_rez1_snr2_0425_0552_nm_r2_1em9	1	0	123.2	2	4.68E-09	4.24E-09	425-552	1
sister_R01_v1_rez1_snr3_0425_0552_nm_r2_1em9	1	0	120.4	3	4.47E-09	4.04E-09	425-552	1
sister_R01_v1_rez1_snr3_0615_0800_nm_r2_1em9	1	0	121.3	3	3.95E-09	5.25E-09	615-800	1
sister_R01_v2_rez1_snr3_0425_0552_nm_r2_1em9	1	-90	177.9	3	2.19E-09	1.99E-09	425-552	2
sister_R01_v2_rez1_snr3_0425_0552_nm_r2_1em9	2	0	295.5	3	7.66E-10	6.95E-10	425-552	2
sister_R01_v2_rez1_snr3_0615_0800_nm_r2_1em9	1	-90	187.2	3	1.79E-09	2.25E-09	615-800	2
sister_R01_v2_rez1_snr3_0615_0800_nm_r2_1em9	2	0	296.0	3	7.72E-10	8.01E-10	615-800	2
sister_R02_v1_rez1_snr3_0425_0552_nm_r2_1em9	1	0	120.5	3	8.20E-09	7.51E-09	425-552	1
sister_R02_v1_rez1_snr3_0615_0800_nm_r2_1em9	1	0	120.0	3	7.18E-09	9.47E-09	615-800	1
sister_R02_v2_rez1_snr3_0425_0552_nm_r2_1em9	1	-90	176.6	3	4.51E-09	4.22E-09	425-552	2
sister_R02_v2_rez1_snr3_0425_0552_nm_r2_1em9	2	0	301.1	3	1.47E-09	1.33E-09	425-552	2
sister_R02_v2_rez1_snr3_0615_0800_nm_r2_1em9	1	-90	189.2	3	3.54E-09	4.56E-09	615-800	2
sister_R02_v2_rez1_snr3_0615_0800_nm_r2_1em9	2	0	298.3	3	1.24E-09	1.49E-09	615-800	2

3.5 Modeling the Disks

The disk emission seen in the simulated images comes in many shapes and sizes. Officially, the exozodi emission is considered “smooth” but there could be resonant features of the dust thus breaking some of the symmetrical distributions of the emission. Forward scattering by the dust grains has also been included into the dust models. While the two epoch subtraction method does a good job of removing the zodiacal emission, it does nothing to characterize the disk itself. For this aspect of the project, we used the IDL ZODIPIC disk simulation code (Kuchner 2012). At the moment, our best fitting models are mostly for the primarily face-on disks as shown in Figure 7. Table 3 lists the planet and disk properties derived from the application of this code on the simulations of tau Ceti (R01, R02). In this case, we provide both the properties of the planets from centroids and the same aperture photometry mentioned previously. Additionally, we list the parameters given to ZODIPIC to produce the disk image. In addition to the physical parameters listed, the program, which accounts for the provided stellar properties, also provides the ratio of the disk flux to star flux (Ld/L_*). For this investigation the disk properties were manipulated manually, and the best fitting disk was determined from the lowest level of a standard deviation taken within an annulus with an inner radius of 4 pixels and outer radius of 15 pixels. Doing this “by eye” was not ideal or efficient given the multiple free parameters in the disk properties so this investigation will be continued as described in the future work section. We did attempt to fit an edge-on disk and a somewhat inclined disk with ZODIPIC but we were not content with the quality of the fits.

Figure 7: Images of the tau Ceti simulation (R01, V1, sez1, 425-552nm, snr3) (upper left) as well as a ZODIPIC model chosen by eye and convolved with the telescope PSF (upper right). Lower left is the combination of the PSF and the ZODIPIC added together and scaled to best match the image. Lower right is the subtraction of the PSF+disk model showing some residual emission from the planet. This scenario shows a clear over subtraction of the model but the intent is to show how the planet emission becomes more apparent after model subtraction.

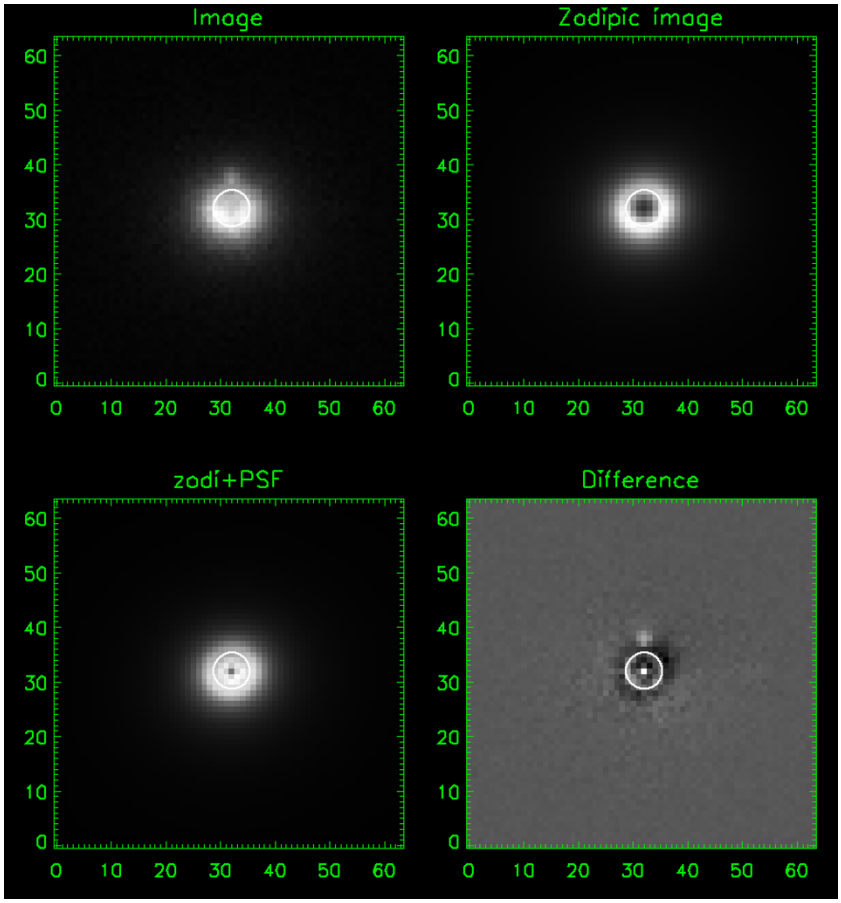

sister_R01_v1_sez1_snr3_0425_0552_nm_r2_1em9

Table 2: Planet properties from those images with Exo-zodi emission and epoch subtraction

Disk/Planet Properties	Disk	Disk		Planet	Planet	Planet Flux
Filename	Morphology	inclination	Wavelength	SMA [mas]	PA	Ratio
sister_R01_v1_sez1_snr3_0425_0552_nm_r2_1em9	smooth	face on	425-552	126.7	0	7.33E-10
sister_R01_v1_sez1_snr3_0615_0800_nm_r2_1em9	smooth	face on	615-800	127.4	0	6.95E-10
sister_R04_v1_sez3_snr3_0425_0552_nm_r2_1em9	smooth	edge on	425-552	87.4	-80	2.00E-09
sister_R04_v1_sez3_snr3_0615_0800_nm_r2_1em9	smooth	edge on	615-800	107.2		1.76E-09
sister_R09_v1_rez3_snr3_0425_0552_nm_r2_1em9	clumpy	45	425-552	seems to be a moving dust feature		
sister_R09_v1_rez3_snr3_0615_0800_nm_r2_1em9	clumpy	45	615-800			
sister_R08_v1_rez3_snr3_0425_0552_nm_r2_1em9	smooth	45	425-552	73.1	-100	1.14E-09
sister_R08_v1_rez3_snr3_0615_0800_nm_r2_1em9	smooth	45	615-800	102.1	-100	9.12E-10
sister_R03_v1_sez3_snr3_0425_0552_nm_r2_1em9	smooth	face on	425-552	144.5	0	2.34E-09
sister_R03_v1_sez3_snr3_0615_0800_nm_r2_1em9	smooth	face on	615-800	143.4	0	2.08E-09
sister_R02_v1_rez3_snr3_0425_0552_nm_r2_1em9	clumpy	face on	425-552	128.2	0	7.35E-09
sister_R02_v1_rez3_snr3_0615_0800_nm_r2_1em9	clumpy	face on	615-800	121.5	0	7.30E-09

Table 3: Planet properties from those images with Exo-zodi emission and ZODIPIC model subtraction

Disk/Planet Properties	Disk	Disk			Planet	Planet	Planet Flux	Disk
Filename	Morphology	inclination	Wavelength	Epoch	SMA [mas]	PA	Ratio	Properties
sister_R01_v1_sez1_snr3_0425_0552_nm_r2_1em9	smooth	face on	425-552	1	138.6	0	1.63E-09	inc=25,rin=0.25 AU, rout=5 AU, PA = -105
sister_R01_v2_sez1_snr3_0425_0552_nm_r2_1em9	smooth	face on	425-552	2	181.6,304.0	-90, 0	2.03e-9,7.4e-10	inc=25,rin=0.25 AU, rout=5 AU, PA = -105
sister_R01_v1_sez1_snr3_0615_0800_nm_r2_1em9	smooth	face on	615-800	1	138.5	0	3.82E-09	inc=25,rin=0.35 AU, rout=5 AU, PA = -105
sister_R01_v2_sez1_snr3_0615_0800_nm_r2_1em9	smooth	face on	615-800	2	194.2,296.5	-90, 0	2.5e-9,7.75e-10	inc=25,rin=0.35 AU, rout=5 AU, PA = -105
sister_R02_v1_sez3_snr3_0425_0552_nm_r2_1em9	smooth	face on	425-552	1	137.2	0	1.12E-08	inc=10,rin=0.25 AU, rout=6 AU, PA = -90
sister_R02_v2_sez3_snr3_0425_0552_nm_r2_1em9	smooth	face on	425-552	2	307.7	0	5.38E-09	inc=10,rin=0.25 AU, rout=6 AU, PA = -90
sister_R02_v1_sez3_snr3_0615_0800_nm_r2_1em9	smooth	face on	615-800	1	126.5	0	3.32E-08	inc=10,rin=0.35 AU, rout=6 AU, PA = -90
sister_R02_v2_sez3_snr3_0615_0800_nm_r2_1em9	smooth	face on	615-800	2	130.0	0	3.30E-08	inc=10,rin=0.35 AU, rout=6 AU, PA = -90

4. Future Work

Given the small timeframe for this investigation, there are components of our analysis which we identify can be improved upon over for the planned publication for this investigation as well as for when we get real-world data. For instance, the disk modeling component with ZODIPIC should be further developed to allow for a Bayesian analysis which will use a set of priors on some of the apparent disk properties (i.e. inclination and position angle) and known star properties (i.e. temperature and luminosity) and then perform a full iteration of a suite of disk parameters. The infrastructure to perform that type of analysis would benefit from a python version of ZODIPIC which we are still in the process of developing. Another simple extension of the codes developed thus far would be one to perform an automatic run through all of the simulated images, do the two-epoch subtraction, and then write out the results for an analysis of the remaining planet emission.

We were not able to begin an investigation into the extraction of the spectral data provided by JPL, however, we would like to develop some python code/Jupyter notebooks to attempt this part of the data challenge over the next few months. A visual inspection of the simulated spectroscopic images and the associated slit position suggests that this would have a straightforward analysis. We would use the spectrum of the disk, which can be recreated from ZODIPIC using a cube of images at multiple wavelengths, in addition to the spectrum of the star and a suite of model planetary spectra to use as a guide.

Over the next few months, which include a class-free summer, the PI plans on expanding upon, refining, and then writing up the results of this investigation for a peer-reviewed publication such at PASP or AJ. Recently, the PI mentioned to Marc Kuchner that we are converting the ZODIPIC code to python and they indicated that we would be welcome to publish a paper on the resulting code as no official paper on the IDL code was ever published. Therefore, we will endeavor to also publish a paper based on the new ZODIPIC python code as well as a suite of Python notebooks we will create to demonstrate how to use the code.

5. Summary and Conclusions

This project has turned out to be the precursor to a bigger program to fully analyze a larger portion of the simulated images and complete a suite of python-based programs to be shared with the Starshade community. From our investigation we determined that using multi-epoch differential imaging is an efficient method for determining whether there is visible point source emission in the images. This can either be the first step in estimating the flux and position of the planet or can help guide a separate analysis which includes creating a realistic model of the circumstellar emission in concert with the planetary emission. A subset of the simulated images

contained circumstellar emission which exhibited clumpy or resonant structures which might not be amenable to modeling with ZODIPIC. In a real-world scenario, a realistic model of the disk which includes the dynamics of the circumstellar material may be the best approach to modeling the disk and then using it to constrain the properties of the planet. Figure 8 shows the new image of the AB Aurigae system taken with the Subaru AO system, SCExAO. This image also shows extended emission from an embedded protoplanet. This image shows the asymmetric structure of the outer disk. Like the multi-epoch differential imaging, ZODIPIC could be used to efficiently remove the primary structure of the exo-zodi emission to be able to search or small-scale emission structures and/or planetary point sources. However, it is also clear that before any observations are collected, we must know as much as possible about each system prior to study. Radial velocity and astrometry will be essential to be able to know where the planets are for scheduling observations at the widest planet-star separation. Direct imaging with ground-based AO systems including Subaru, Keck and the VLT will be essential to estimate Ld/L* and map out the outer structure of the disks. The ZODIPIC tool has parameters for grain size and dust disk and temperature structure which would benefit from a priori knowledge when modeling the disk. With all this in mind the key to community engagement will be to create a set of analysis tools which combine the data from all of these methods in a comprehensive characterization of these planetary systems.

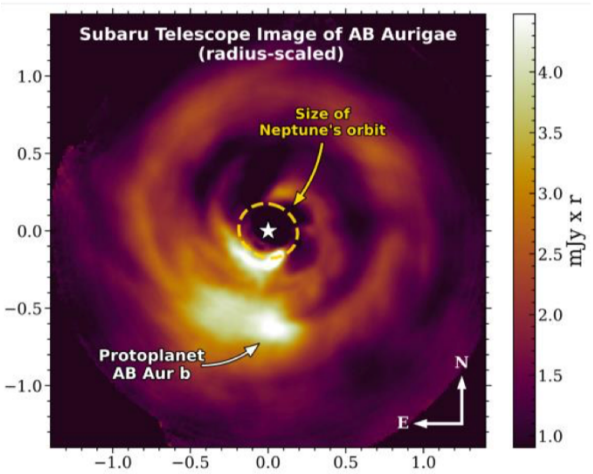

Figure 8: Image of AB Aurigae taken with Subaru showing both the protostellar disk and newly identified protoplanet (Currie et al. 2022).

References

Hildebrandt, S.R., Shaklan, S.B., Cady, E.J., et al. 2022, Astrophysics Source Code Library.
Kuchner, M. 2012, Astrophysics Source Code Library. ascl:1202.002.
Lowrance, P.J., Becklin, E.E., Schneider, G., et al. 2005, AJ, 130, 1845.